Acta Cryst. (1997). B53, 604–612

Structure of Two Disordered Molybdates, $Li_2Mo^{IV}O_3$ and $Li_4Mo_3^{IV}O_8$, from Total Neutron Scattering

SIMON J. HIBBLE,[a]* IAN D. FAWCETT[a] AND ALEX. C. HANNON[b]

[a]*Department of Chemistry, University of Reading, Whiteknights, PO Box 224, Reading RG6 6AD, England, and* [b]*ISIS Facility, Rutherford Appleton Laboratory, Chilton, Didcot, Oxon OX11 0QX, England. E-mail: s.j.hibble@rdg.ac.uk*

(*Received 14 October 1996; accepted 7 March 1997*)

Abstract

The structures of the disordered lithium molybdates Li_2MoO_3 and $Li_4Mo_3O_8$ have been investigated using total neutron scattering from polycrystalline powders. Rietveld analysis of the Bragg scattering is used to determine the average structures. Shortcomings in this method of analysis are demonstrated by comparing the total correlation function, $T(r)$, determined from total neutron scattering, with those calculated from the structures determined from Rietveld analysis. Much more satisfactory models for these materials are derived from the structurally related ordered material $LiZn_2Mo_3O_8$, using information from Mo *K*-edge extended X-ray absorption fine-structure spectroscopy (EXAFS). These models include metal–metal-bonded Mo_3O_{13} clusters [d(Mo—Mo) = 2.58 Å in Li_2MoO_3 and 2.56 Å in $Li_4Mo_3O_8$] not present in the average structure determined from Rietveld analysis [d(Mo—Mo) = 2.88 Å in Li_2MoO_3]. In contrast to EXAFS studies neutron diffraction yields information on all the pair correlations in the material, not merely those involving molybdenum, and allows, for example, the location of lithium. Remaining discrepancies between our models and the experimental $T(r)$'s give an insight into the disorder in the two materials.

1. Introduction

Structural studies using only Bragg scattering neglect a large amount of the information present in the diffraction pattern of a sample. This information is often seen as an unnecessary complication by the chemical crystallographer, who wishes to determine the space group, lattice parameters and atomic parameters for a new compound and to draw the structure and measure interatomic distances. Modelling of diffuse scattering is seen as the realm of the physicist and is especially difficult for powder samples where the three-dimensional information is collapsed into one dimension. The effects of disorder are normally absorbed into temperature factors in the structural model and an average structure is produced. This average structure will of course contain much valuable information and in most instances does not deviate markedly from the real structure.

In some instances modelling only the Bragg scattering is inadequate for the needs of the chemical crystallographer. In this paper we discuss the cases of the intrinsically disordered lithium molybdate Li_2MoO_3 (James & Goodenough, 1988) and the related material $Li_4Mo_3O_8$ (Hibble & Fawcett, 1995), both of which contain metal–metal-bonded Mo_3 clusters. A previous neutron diffraction study of Li_2MoO_3 by James & Goodenough (1988) produced an average structure from a conventional Rietveld analysis of the data, which gave no information on the type of Mo—Mo bonded clusters in this material. They determined that the average structure is built from cubic close-packed oxide layers in which mixed $[Mo_{2/3}Li_{1/3}]O_2$ layers, with the metal atoms in octahedral sites, are interspersed by further lithium ions filling the octahedral sites between the layers. The layer structure is shown in Fig. 1. This material is intrinsically disordered, because the composition of the mixed layers, $[Mo_{2/3}Li_{1/3}]$, does not allow the possibility of forming an ordered arrangement of Mo_3 clusters on a hexagonal lattice. Analogy with other Mo^{IV} systems, for example, $Zn_2Mo_3O_8$ (McCarrol, Katz & Ward, 1957), and evidence from photoelectron spectroscopy (James & Goodenough, 1988) pointed to the presence of Mo_3O_{13} clusters, Fig. 2, and we were able to confirm this using EXAFS studies at the Mo *K*-edge (Hibble & Fawcett, 1995). Fig. 3(*a*) shows an ordered arrangement of Mo atoms in the $Mo_{3/4}O_2$ layer in $Zn_2Mo_3O_8$ and Fig. 3(*b*) (after James & Goodenough, 1988) shows a disordered arrangement of Mo atoms in the $[Mo_{2/3}Li_{1/3}]O_2$ layer with Mo—Mo bonds drawn to represent Mo_3 clusters. Note, however, that the distances between all molybdenum nearest-neighbours in Li_2MoO_3 are identical in this diffraction study (James & Goodenough, 1988).

In our investigation of the Li_2O–MoO_2 phase diagram we discovered the existence of another phase, $Li_4Mo_3O_8$ (Hibble & Fawcett, 1995). Our EXAFS studies showed that this too contained Mo_3 clusters and the powder X-ray pattern showed it to be isostructural with Li_2MoO_3. The similarity of the compounds can be seen by expressing their composition with respect to MO_2 layers. Thus, the formula of Li_2MoO_3 can be expressed as $Li[Mo_{2/3}Li_{1/3}]O_2$ and that of $Li_4Mo_3O_8$ as

$Li[Mo_{3/4}V_{1/4}]O_2$ or $Li_{3/4}V_{1/4}[Mo_{3/4}Li_{1/4}]O_2$ (where V is a vacant octahedral metal site). Although the composition of this compound would appear to allow the formation of ordered layers similar to those found in $Zn_2Mo_3O_8$ ($Zn_{1/2}[Mo_{3/4}]O_2$), Fig. 3(*a*), no evidence for this was seen in the powder X-ray pattern.

To discover more about the structures of these reduced molybdates, we collected total neutron scattering data, since this would allow us to determine the total correlation function, $T(r)$. This contains information on all interatomic vectors, not merely those around the probe atom, as from EXAFS experiments, and also extends to much greater distances. Our goal was to produce structural models including metal–metal-bonded Mo_3O_{13} clusters, which would account for all the neutron scattering and hence improve on the previous model for Li_2MoO_3 derived from Bragg scattering.

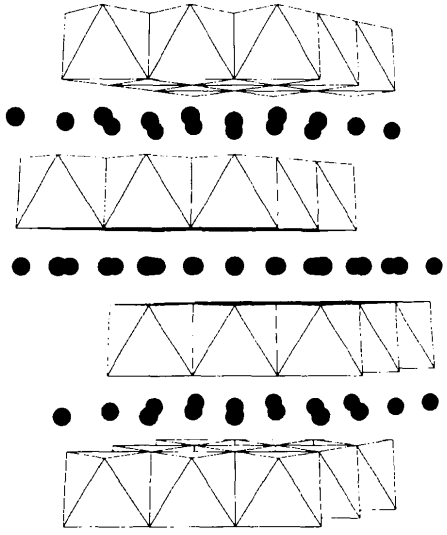

Fig. 1. The Li_2MoO_3 layered structure. Octahedra form $[Mo_{2/3}Li_{1/3}]O_2$ layers, shaded circles denote interlayer Li atoms.

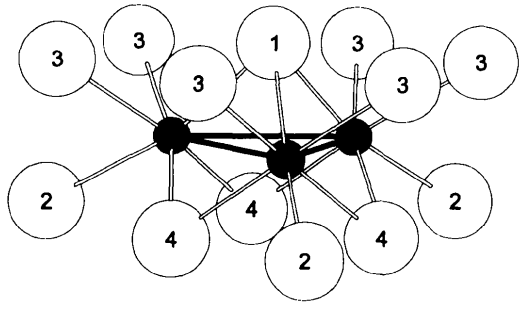

Fig. 2. A Mo_3O_{13} cluster (solid circles, Mo; open circles, O); O atoms are labelled in accordance with the numbering scheme used in Tables 3 and 4.

2. Theory

The basic quantity measured in neutron diffraction is the differential cross section (Hannon, Howells & Soper, 1990)

$$d\sigma/d\Omega = I(Q) = I^s(Q) + i(Q), \quad (1)$$

where $I^s(Q)$ is known as the self-scattering and $i(Q)$ is known as the distinct scattering. Q is the magnitude of the scattering vector (momentum transfer) for elastic scattering, given by

$$Q = (4\pi \sin\theta)/\lambda. \quad (2)$$

After subtracting the self-scattering the distinct scattering is Fourier transformed to give the total correlation function $T(r)$

$$T(r) = T^0(r) + (2/\pi \int_0^\infty Qi(Q)M(Q)\sin(rQ)dQ \quad (3)$$

$$T^0(r) = 4\pi r g^0(\sum_l c_l \bar{b}_l)^2, \quad (4)$$

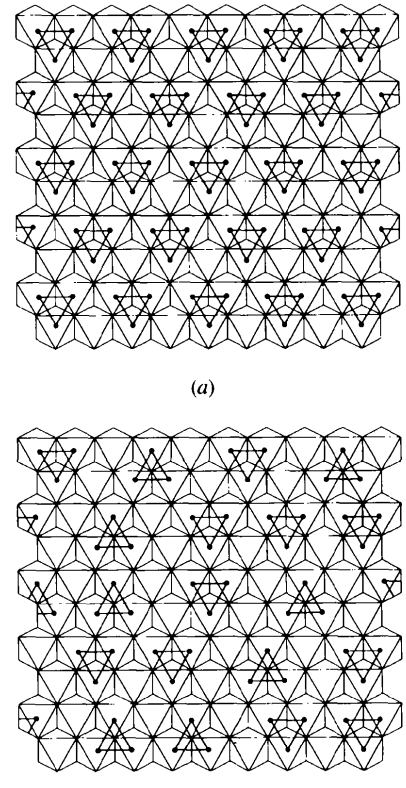

(*a*)

(*b*)

Fig. 3. (*a*) Ordered Mo_3 triangles in the $[Mo_{3/4}]O_2$ layers in $Zn_2Mo_3O_8$; (*b*) disordered Mo_3 triangles in the $[Mo_{2/3}Li_{1/3}]O_2$ layers in Li_2MoO_3 (solid circles, Mo).

where $M(Q)$ is a modification function (used to take into account that the diffraction pattern is measured up to a finite momentum transfer Q_{max} and not to infinity), $g^o(= N/V)$ is the macroscopic number density of scattering units, c_l is the atomic fraction and $\bar{b}_l$ the coherent neutron scattering length for element l. The modification function is a step function cutting off at $Q = Q_{max}$ and the one used is that due to Lorch (1969)

$$M(Q) = [\sin(Q\Delta r)/Q\Delta r] \text{ for } Q < Q_{max} \quad (5)$$

$$= 0 \text{ for } Q > Q_{max}, \quad (6)$$

where $\Delta r = \pi/Q_{max}$.

To calculate $T(r)$ we employed the program *Xtal* (Hannon, 1993) and the *GENIE* (David *et al.*, 1986) input program *RDF* (Hannon, 1993). *Xtal* produced the partial pair distribution functions $g_{ll'}$ from the atomic and lattice parameters of our model

$$g_{ll'}(r) = \left(1/\sum_{i=1}^{N_l} w_i\right) \sum_{j=1}^{N_l} \sum_{j'=1}^{N_{l'}} w_j w_{j'} < \delta(\mathbf{r} + \mathbf{R}_j - \mathbf{R}_{j'}) >, \quad j \neq j' \quad (7)$$

$j \neq j'$, where $\mathbf{R}_j$ is the position of the jth atom and w_i is the occupancy of the ith atom. The j, j' sums are over the $N_l, N_{l'}$ atoms of element l, l' and $j \neq j'$ indicates that j and j' are not allowed to refer to the same atom. $g_{ll'}$ may be interpreted as the number density of atoms of element l' at a distance r (= $|r|$) from an origin atom of element l, averaged over all possible origin atoms and directions of $\mathbf{r}$. The weighted partial correlation functions $t_{ll'}$

$$t_{ll'}(r) = 4\pi r g_{ll'}(r) \quad (8)$$

were then summed to yield the total correlation function $T(r)$

$$T(r) = \sum_{ll'} c_l \bar{b}_l \bar{b}_{l'} t_{ll'}(r), \quad (9)$$

where c_l (= N_l/N) is the atomic fraction for element l and the l and l' summations are both over the elements of the sample. The functions $t_{ll'}(r)$ and $T(r)$ were broadened using a Gaussian function to simulate the broadening of experimental data due to thermal motion and finite resolution in real space. This function

$$P(r) = 1/[\sigma(2\pi)^{1/2}]\exp[(r - r_0)^2/2\sigma^2] \quad (10)$$

preserved coordination numbers.

3. Experimental

3.1. *Sample preparation and characterization*

$^7Li_2MoO_4$ and $^7Li_4MoO_5$ were prepared from stoichiometric quantities of $^7Li_2CO_3$ (99.95 atom% ^7Li) and MoO_3, ground together and heated at 823 K for 24 h in an alumina crucible. $^7Li_2MoO_3$ was prepared from $^7Li_4MoO_5$, MoO_3 and Mo powder, mixed in the required stoichiometric ratios and pressed into pellets in an alumina crucible contained in a sealed evacuated silica tube. The mixture was heated for 24 h at 773 K and then held at 1173 K for 4 d. $^7Li_4Mo_3O_8$ was prepared from $^7Li_2MoO_4$ and Mo powder by the same method. Powder X-ray diffraction patterns of the products were recorded using a Spectrolab Series 3000 CPS-120 X-ray diffractometer equipped with an INEL multichannel detector. The diffraction patterns of the samples matched those given in the literature (James & Goodenough, 1988; McGrellis, 1994).

3.2. *Data collection*

Time-of-flight powder neutron diffraction data were collected on the LAD diffractometer at ISIS, Rutherford Appleton Laboratory, Chilton, Didcot, England (Howells, 1980). LAD is equipped with pairs of detector banks at 5, 10, 20, 35, 58, 90 and 150°. Approximately 5 g of powdered molybdate was loaded into a cylindrical 8 mm diameter vanadium sample holder. The effective density of each sample, as used in the data correction routines, was determined from the sample depth and exact mass used. Samples were cooled to 12–13 K using a closed cycle refrigerator. Data were collected over the time-of-flight range 100–19 750 μs (Q range 0–50 $Å^{-1}$). Background runs were collected on the empty can and empty spectrometer, and data were collected for a standard vanadium rod.

4. Data reduction and analysis

4.1. *Rietveld analysis*

Data for Rietveld analysis were obtained by combining the signals from the two 150° detector banks and normalizing to the neutron flux. Standard Rietveld refinements for both Li_2MoO_3 and $Li_4Mo_3O_8$ were carried out using the program *TF12LS* (David, Ibberson & Matthewman, 1992), over the d-space range 0.46–3.55 Å, with the peak shape modelled by a pseudo-Voigt function convoluted with a double exponential function. The coherent scattering lengths used for ^7Li, Mo and O were -0.22×10^{-14}, 0.69×10^{-14} and 0.5805×10^{-14} m, respectively (Koester & Yelon, 1982). James & Goodenough's (1988) model for Li_2MoO_3 was used as a starting point for the refinements. In the case of $Li_4Mo_3O_8$, the mixed Mo/Li layer was replaced by a fractionally (3/4) occupied molybdenum layer to achieve the correct composition. The scale and five polynomial background parameters were refined first, followed by the unit cell, the atomic parameters, the independent temperature factors and finally the peak parameters. The refined lattice and atomic parameters are given in Tables 1 and 2, and I_{obs}, I_{calc} and the

Table 1. *Fractional atomic coordinates and equivalent isotropic displacement parameters (Å^2) for Li_2MoO_3*

$$B_{eq} = (1/3)\Sigma_i\Sigma_j B^{ij} a_i^* a_j^* \mathbf{a}_i.\mathbf{a}_j.$$

	Site	x	y	z	B_{eq}
Li1*	3(*b*)	0.0	0.0	1/2	1.23 (9)
Mo†	3(*b*)	0.0	0.0	1/2	1.23 (9)
Li2	3(*a*)	0.0	0.0	0.0	1.2 (1)
O	6(*c*)	0.0	0.0	0.2450 (1)	0.60 (3)

* Occupancy 1/3. † Occupancy 2/3. Space group = $R\bar{3}m$, a = 2.878 (7), c = 14.9119 (4) Å, number of reflections used in the refinement = 172, $\chi^2 = (R_{wp}/R_{ex})^2$ = 1551.3 for 2541 observations and 16 basic variables, $R_{wp} = [\Sigma_i w_i|Y_i(\text{obs}) - Y_i(\text{calc})|^2]^{1/2}$ = 0.1017, $R_{ex} = [(N - P + C)/\Sigma_i w_i Y_i(\text{obs})^2]^{1/2}$ = 0.0026; R_{wp} is the weighted profile R factor, R_{ex} is the expected R factor, w_i is the weight for point i, N is the number of observations, Y_i is the intensity of point i, P is the number of variables and C is the number of constraints.

Table 2. *Fractional atomic coordinates and equivalent isotropic displacement parameters (Å^2) for $Li_4Mo_3O_8$*

$$B_{eq} = (1/3)\Sigma_i\Sigma_j B^{ij} a_i^* a_j^* \mathbf{a}_i.\mathbf{a}_j.$$

	Site	x	y	z	B_{eq}
Mo*	3(*b*)	0.0	0.0	1/2	1.67 (9)
Li	3(*a*)	0.0	0.0	0.0	5.8 (4)
O	6(*c*)	0.0	0.0	0.2421 (2)	0.76 (4)

* Occupancy 3/4. Space group = $R\bar{3}m$, a = 2.8688 (5), c = 15.3843 (4) Å, number of reflections used in the refinement = 175, χ^2 = 1816.5 for 2541 observations and 16 basic variables, R_{wp} = 0.1430, R_{ex} = 0.0034.

difference plots are shown in Fig. 4.* The parameters for Li_2MoO_3 are in excellent agreement with those of James & Goodenough (1988), but it is clear from Fig. 4(*a*) that the structure refinement gives rather a poor fit to the experimental data. Two weak peaks from Li_2CO_3 impurities ($\sim$ 3%) can be seen at d= 2.64 and 2.81 Å. No significant improvement is made to the refinement by excluding these. The structural refinement for $Li_4Mo_3O_8$, Fig. 4(*b*), is of similar quality, although in this case a number of broad reflections not included in the model are seen (at $d \simeq$ 2.87 and 2.31 Å and peaks around d = 1.79 Å). These are not due to impurities and their origin is discussed later. These results demonstrate that the average structures illustrated in Fig. 1, and described in the *Introduction*, are correct and that $Li_4Mo_3O_8$ is isostructural with Li_2MoO_3. The relatively poor agreement of the observed and calculated profiles show that problems remain in the description of the structures. Attempts to improve the fits by allowing molybdenums to move onto more general positions, which would give shorter Mo—Mo distances typical of Mo_3 clusters, did not produce a statistically significant improvement. The quality of agreement of the observed and calculated profiles shows that, whilst the average long-range structures are correct, problems remain in describing short-range order.

* The numbered intensity of each measured point on the profile and the primary diffraction data, also merged to total neutron scattering, have been deposited with the IUCr (Reference: AB0367). Copies may be obtained through The Managing Editor, International Union of Crystallography, 5 Abbey Square, Chester CH1 2HU, England.

4.2. *Total neutron scattering*

Data for total neutron scattering were obtained by merging the data from all 14 detector banks (over the Q range 0–30 Å^{-1}) normalized to absolute scattering units, after correcting for detector deadtime, multiple scattering, inelasticity and attenuation using the *ATLAS* suite of programs (Soper, Howells & Hannon, 1989).

The interference function, $Qi(Q)$, for Li_2MoO_3 and $Li_4Mo_3O_8$, out to Q = 30 Å^{-1}, is shown in Fig. 5. The Li_2MoO_3 data were corrected for the presence of a small amount ($\sim$ 3%) of Li_2CO_3 by subtracting appropriate fractions of identically normalized data collected on pure Li_2CO_3.

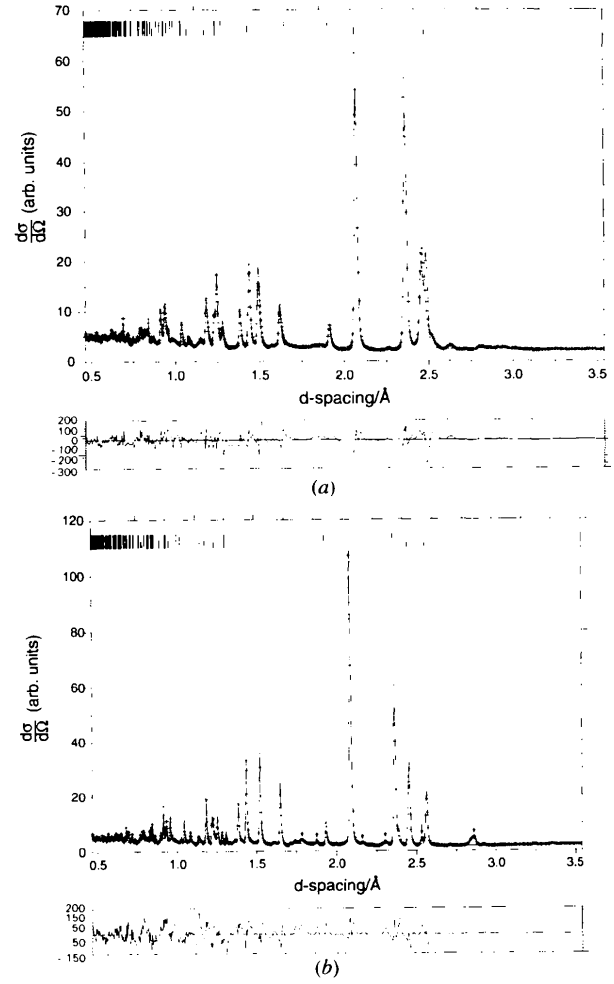

Fig. 4. Final fitted profiles (observed, points; calculated; line; difference, lower) from Rietveld refinements for (*a*) Li_2MoO_3 using the James & Goodenough (1988) model and (*b*) $Li_4Mo_3O_8$ (note broad superlattice peaks for $Li_4Mo_3O_8$, indicated by vertical arrows).

5. Modelling

The total correlation function, $T(r)$, from 0 to 7 Å, obtained by Fourier transforming $Qi(Q)$ according to equation (3) for Li_2MoO_3 is shown in Fig. 6(*a*) along with that calculated from the average structure given in Table 1. Fig. 6(*a*) shows clearly that the short- and medium-range structure in Li_2MoO_3 is poorly modelled by the structural model given in Table 1. A similar plot for $Li_4Mo_3O_8$ is shown in Fig. 6(*b*). This disagreement was not unexpected, since we knew from EXAFS studies (Hibble & Fawcett, 1995) that these materials contained Mo_3 clusters. To produce a model which would give a better representation of the short- and medium-range structure in these materials presents a problem, since extremely large models containing hundreds of atoms are required if distances up to 7 Å are to be modelled. We decided to employ ordered models and retain crystallographic symmetry in our attempt to fit $T(r)$, since this reduced the complexity of the problem and the number of variables. We believe the following results justify this apparently perverse method of modelling disordered materials.

5.1. *The Mo—O framework of Li_2MoO_3 and $Li_4Mo_3O_8$*

We searched the literature for suitable Mo_3 cluster compounds to act as starting models. The compound

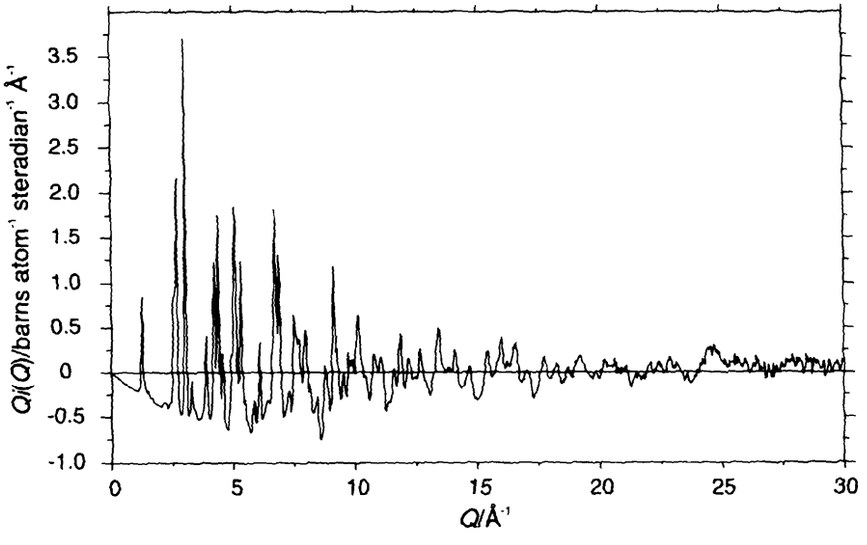

(*a*)

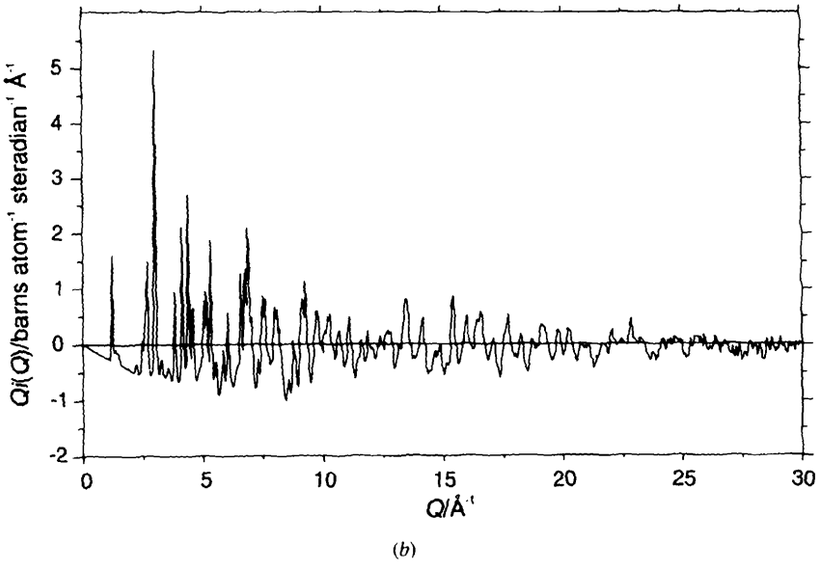

(*b*)

Fig. 5. The interference function $Qi(Q)$ for (*a*) Li_2MoO_3 and (*b*) $Li_4Mo_3O_8$.

$LiZn_2Mo_3O_8$ (Torardi & McCarley, 1985), space group $R\bar{3}m$, proved suitable. This compound has unit-cell parameters which are approximately double those of Li_2MoO_3 and $Li_4Mo_3O_8$. The doubling of a and b allows Mo_3 clusters to be formed simply by displacing Mo from the special positions in Li_2MoO_3 and $Li_4Mo_3O_8$, and the doubling of c retains the approximately close-packed oxide layers when oxygens are displaced from the idealized positions in the average Li_2MoO_3 and $Li_4Mo_3O_8$ structures described above. To produce our models we doubled the lattice parameters from our refinements for Li_2MoO_3 and $Li_4Mo_3O_8$ obtained above. We placed Mo on x, $\bar{x}$, z positions and fixed x at values which gave Mo—Mo distances in agreement with our EXAFS studies (Hibble & Fawcett, 1995). We then adjusted the atomic parameters for oxygen from those found for $LiZn_2Mo_3O_8$ to give the Mo—O distances found in the EXAFS studies of Li_2MoO_3 and $Li_4Mo_3O_8$. The correlation functions, $T(r)$, for these models were calculated using the *Xtal* program described above, with the histogram of interatomic distances broadened using a Gaussian of width 0.1 Å to account for thermal vibrations and real-space resolution. These models, which did not yet include Li atoms, produced calculated $T(r)$'s with overall forms closer to the experimentally determined $T(r)$'s than those produced by the average structures. The next step was to add lithium to our models.

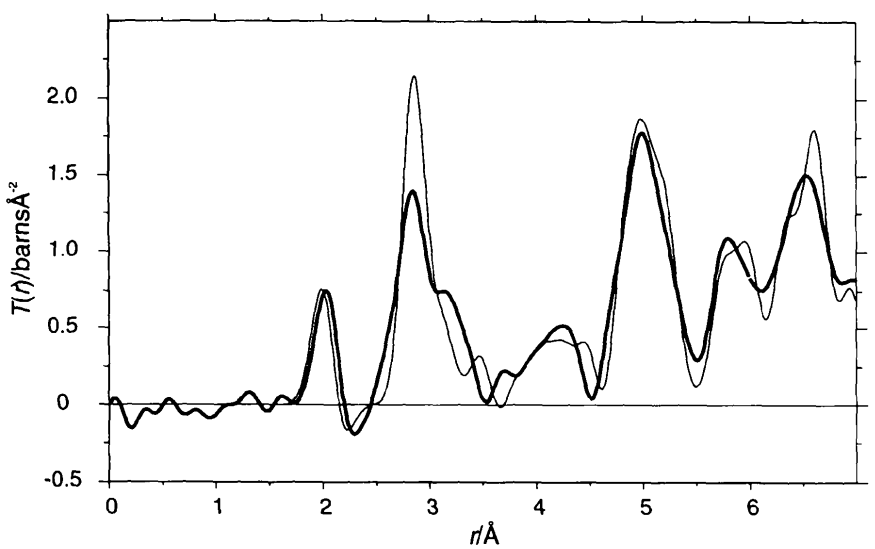

(*a*)

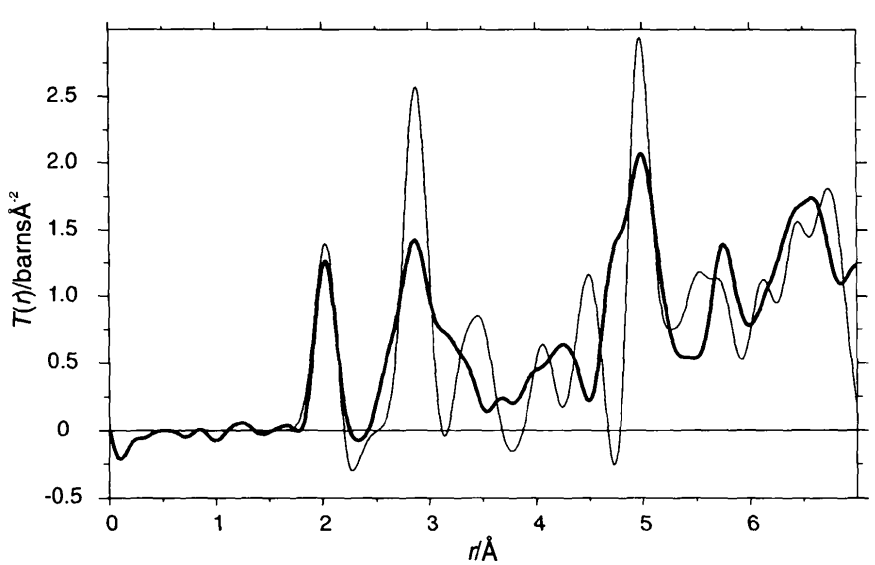

(*b*)

Fig. 6. (*a*) $T(r)_{exp}$ (heavy line) and $T(r)$ calculated for the average structure from Rietveld refinement for Li_2MoO_3 (light line), and (*b*) $T(r)_{exp}$ (heavy line) and $T(r)$ calculated for the average structure from Rietveld refinement for $Li_4Mo_3O_8$ (light line).

Table 3. *$Li_4Mo_3O_8$ model for $T(r)$ calculation*

	Site	x	y	z
Mo	18(*h*)	0.1846	0.8154	0.0839
O1	6(*c*)	0.0	0.0	0.3738
O2	6(*c*)	0.0	0.0	0.1182
O3	18(*h*)	0.8454	0.1546	0.0479
O4	18(*h*)	0.4941	0.5059	0.1230
Li1	6(*c*)	0.0	0.0	0.1803
Li2	6(*c*)	0.0	0.0	0.3080
Li3	3(*a*)	0.0	0.0	0.0
Li4	3(*b*)	0.0	0.0	1/2
Li5*	18(*h*)	2/3	1/3	0.0894

* Occupancy 1/3. Space group $R\bar{3}m$ (hexagonal setting), a = 5.738, c = 30.768 Å, $R = \Sigma_i|Y_i(\text{obs}) - Y_i(\text{calc})|^2 / \Sigma_i Y_i(\text{obs})^2]^{1/2}$ (over the fit range 1.5–7.0 Å) = 0.1756 [R for average structure (parameters in Table 2) = 0.3620].

5.2. *$Li_4Mo_3O_8$*

We tried two possible models for $Li_4Mo_3O_8$. In model 1 we placed all the lithium on octahedral sites between the $[Mo_{0.75}O_2]$ layers. In model 2 we placed lithium on octahedral and tetrahedral sites derived from the Li and Zn sites in $LiZn_2Mo_3O_8$ and added extra Li atoms in the vacant octahedral positions in the lithium layer to achieve the correct composition. Model 2 can be formulated as $(Li_{tet})_2Li_{oct}[(Mo_{oct})_{0.75}(Li_{oct})_{0.25}O_2]$. Model 2 gave a significantly better fit to $T(r)$ (R = 0.177 defined in Table 3) than model 1 (R = 0.242); both were much better than the Rietveld model (R = 0.362). The calculated $T(r)$ for model 2 is compared with the experimentally determined $T(r)$ for $Li_4Mo_3O_8$ in Fig. 7, together with the partial correlation functions. In spite of its low neutron scattering length, the positioning of lithium has a dramatic impact on the calculated $T(r)$. This is due to the large contribution of the Li—O partial correlation function to $T(r)$ (negative $\bar{b}_l$ is an advantage). The atomic parameters for this model are given in Table 3. Fig. 8 shows the structure.

5.3. *Li_2MoO_3*

The correct composition for Li_2MoO_3 can only be achieved by placing lithium on octahedral sites within and between the $[Mo_{2/3}O_2]$ layers. In Fig. 9 the calculated $T(r)$ for this model is compared with the experimentally determined $T(r)$ for Li_2MoO_3 together with the partial correlation functions. The atomic parameters for this model are given in Table 4. This model clearly gives a better fit to $T(r)$ (R = 0.214) than the average structure derived from Rietveld analysis (R = 0.300).

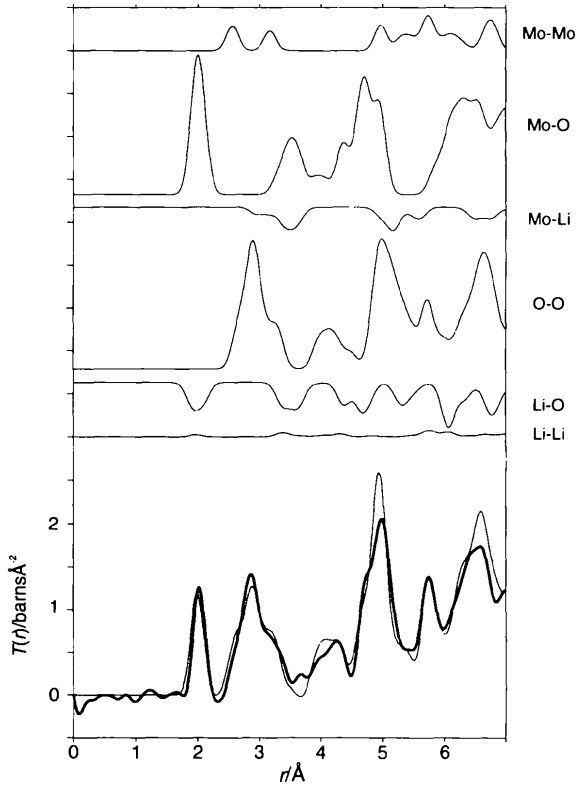

Fig. 7. Bottom: $T(r)$ exp (heavy line) and $T(r)$ calculated for our model (Table 3) for $Li_4Mo_3O_8$ (light line); above: contributions from the partials, $t_{ll}(r)$.

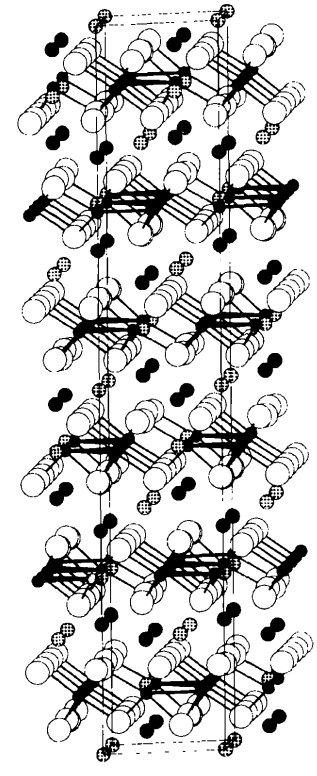

Fig. 8. Structural model for $Li_4Mo_3O_8$ as seen along the b axis (small solid circles, Mo; large open circles, O; lightly shaded circles, tetrahedral Li; spotted heavily shaded circles, octahedral Li), light lines indicate the unit cell.

6. Discussion

6.1. $Li_4Mo_3O_8$

The possible formulations derived from the average structure for Li_2MoO_3, $Li[Mo_{3/4}V_{1/4}]O_2$ or $Li_{3/4}V_{1/4}[Mo_{3/4}Li_{1/4}]O_2$ (where V is a vacant octahedral metal site) did not suggest any structural reason for the existence of a phase with this particular composition on the Li_2O–MoO_2 tie line. The composition of $Li_4Mo_3O_8$ is now understandable, since it represents full occupancy of a set of octahedral and tetrahedral sites giving the structural formula $(Li_{tet})_2Li_{oct}[(Mo_{oct})_{0.75}(Li_{oct})_{0.25}O_2]$.

Simulation of the Bragg scattering using the atomic parameters of our model for $Li_4Mo_3O_8$ given in Table 3 gave peaks in the correct positions. The fit to the subcell reflections gives similar agreement to that obtained earlier using the average model. These peaks are sharp and their widths reasonably modelled. The other reflections arising from ordering are broad and their intensities and widths are poorly modelled. The positions of a number of these broad peaks are indicated in Fig. 4(*b*), the most obvious is the 110 (indexed on the supercell) reflection just below 3 Å. We ascribe the large peak widths of these supercell reflections to disorder in the form of stacking faults along **c**. In this material the Mo_3O_{13} clusters appear to be ordered in $Mo_{3/4}O_2$ layers, as in $Zn_2Mo_3O_8$, but with disorder in registry between these layers. This can be explained by the presence of the interlayer cations, Li^+, in $Li_4Mo_3O_8$ with a smaller charge and less rigid bonding requirements than the interlayer cations, Zn^{2+}, in $Zn_2Mo_3O_8$.

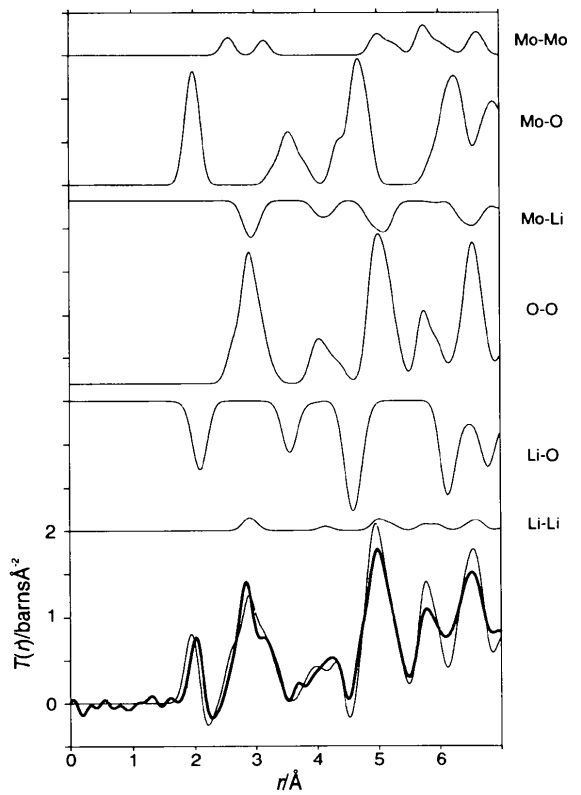

Fig. 9. Bottom: $T(r)_{exp}$ (heavy line) and $T(r)$ calculated for our model (Table 3) for Li_2MoO3 (light line); above: contributions from the partials, $t_{ll'}(r)$.

Table 4. *Li_2MoO_3 model for $T(r)$ calculation*

	Site	x	y	z
Mo*	18(*h*)	0.1836	0.8164	0.0839
O1	6(*c*)	0.0	0.0	0.3730
O2	6(*c*)	0.0	0.0	0.1170
O3	18(*h*)	0.8454	0.1546	0.0456
O4	18(*h*)	0.4941	0.5059	0.1229
Li1	3(*a*)	0.0	0.0	0.0
Li2	3(*b*)	0.0	0.0	1/2
Li3	9(*d*)	1/2	0.0	1/2
Li4	(*e*)	0.0	1/2	0.0
Li5†	18(*h*)	0.1580	0.8420	0.0839
Li6‡	18(*h*)	0.6697	0.3303	0.0830

* Occupancy 8/9. † Occupancy 1/9. ‡ Occupancy 1/3. Space group $R\bar{3}m$ (hexagonal setting), a = 5.755, c = 29.824 Å, R = 0.2140 [R for James & Goodenough (1988) model (parameters in Table 1) = 0.300].

Modelling Rietveld data with *hkl*-dependent line broadening is difficult and requires a good structural model as the starting point. Modelling of total neutron scattering provides another approach to data analysis and a route to a starting model for such studies. In the present case we have obtained the structural information we desired, the structure of the Mo—Mo bonded clusters, from total neutron scattering, and we have not pursued Rietveld modelling further.

6.2. Li_2MoO_3

Although the model for Li_2MoO_3 produced above gives a better fit to $T(r)$ than the average structure derived from Rietveld analysis, the overall agreement is poorer than that for $Li_4Mo_3O_8$, see Fig. 9. The poor agreement of the first peak at ~ 2 Å between the calculated and experimentally determined $T(r)$ is at first sight surprising, especially since this peak appears to be fitted well by the average structure. However, close inspection of the contributions of the partial $t_{ll}(r)$'s shows that the agreement of $T(r)$ from the average structure is fortuitous. It arises because the Mo—O distances, which are known to be in error (Hibble & Fawcett, 1995), produce a positive peak in $t(r)_{Mo-O}$ at an almost identical r to the negative peak in $t_{Li-O}(r)$.

Inspection of the contributions made by the various $t_{ll}(r)$'s to $T(r)$ suggests that the molybdenum–oxygen framework in this model is now a much closer representation of the real structure of Li_2MoO_3 than the average structure derived from Bragg scattering. The most significant remaining discrepancies in $T(r)$ can be ascribed to problems modelling disorder with an ordered model. The problems with the first peak in $T(r)$ arise from poor modelling of lithium–oxygen distances. This is not surprising, since lithium can easily adapt to

various coordination geometries and probably moves off the idealized positions in this model to compensate for lithium replacing molybdenum in the mixed Mo/Li layer. The peaks in $T(r)_{calc}$ between 4.5 and 7 Å are sharper than those in $T(r)_{exp}$, due to disorder in the Mo—O framework, which we have not yet modelled, and the effects of instrumental Q-resolution, which dampen the oscillations in $T(r)$, particularly at higher r.

For Li_2MoO_3 no improvement in the Rietveld fit was achieved using the new model and there is no evidence in the Bragg scattering of any long-range order arising from the formation of Mo_3 triangles. In this case total neutron scattering and modelling $T(r)$ supplies extra information not available from Bragg scattering.

7. Conclusions

Total neutron scattering studies have yielded information on both the short- and long-range order in Li_2MoO_3 and $Li_4Mo_3O_8$. A model derived from the ordered material, $LiZn_2Mo_3O_8$, using information from EXAFS studies has been shown to give a much better description of the short-range order in $Li_4Mo_3O_8$ than that obtained using the average unit cell and it clearly demonstrates the presence of Mo—Mo-bonded Mo_3O_{13} clusters in this compound. The explanation for the disorder is the existence of stacking faults. This conclusion is supported by the presence of broad peaks in the powder diffraction pattern at positions predicted by the larger unit cell of our model, but not accounted for by the sub-cell obtained from the sharp Bragg peaks.

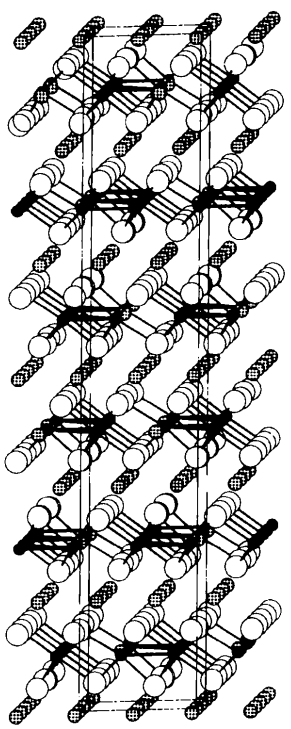

Fig. 10. Structural model for Li_2MoO_3, as seen along the b axis (small solid circles, Mo; large open circles, O; spotted circles octahedral, Li), light lines indicate the unit cell.

The presence of Mo_3O_{13} clusters in Li_2MoO_3 has also been demonstrated by modelling $T(r)$ in the same manner as $Li_4Mo_3O_8$. The inadequacy of a model which fits only Bragg scattering from intrinsically disordered Li_2MoO_3 and, therefore, neglects the formation of disordered metal–metal-bonded Mo_3O_{13} clusters has been demonstrated. The remaining discrepancies between the calculated and experimentally derived $T(r)$ can be accounted for by disorder in the lithium positions.

We suggest that the calculation and modelling of $T(r)$ using neutron scattering data from disordered crystalline as well as from amorphous materials is extremely useful. It can reveal problems and inadequacies in the model being used to fit the Bragg diffraction data and also reveal structural information not contained in a model of the average structure. It can be used whatever the cause of disorder and aid in the elucidation of the mechanisms of disorder.

We thank the EPSRC for the provision of neutron diffraction facilities and a studentship for IDF.

References

David, W. I. F., Ibberson, R. M. & Matthewman, J. C. (1992). Report RAL-92-032. Rutherford Appleton Laboratory, Didcot, Oxford, England.

David, W. I. F., Johnson, M. W., Knowles, K. J., Moreton-Smith, C. M., Crosbie, G. D., Campbell, E. P., Graham, S. P. & Lyall, J. S. (1986). Report RAL-86-102. Rutherford Appleton Laboratory, Didcot, Oxford, England.

Hannon, A. C. (1993). Report RAL-93-063. Rutherford Appleton Laboratory, Didicot, Oxford, England.

Hannon, A. C., Howells, W. S. & Soper, A. K. (1990). In *Proceedings of the Second Workshop on Neutron Scattering Data Analysis* (*WONSDA2*), edited by M. W. Johnson, Conference Series 107, pp. 193–211. Bristol: IOP.

Hibble, S. J. & Fawcett, I. D. (1995). *Inorg. Chem.* **34**, 500–508.

Howells, W. S. (1980). Report RAL-80-017. Rutherford Appleton Laboratory, Didcot, Oxford, England.

James, A. C. W. P. & Goodenough, J. B. (1988). *J. Solid State Chem.* **76**, 87–96.

Koester, L. & Yelon, W. B. (1982). *Summary of Low Energy Neutron Scattering Lengths and Cross Sections*. Netherland Research Foundation, Department of Physics, Petten, The Netherlands.

Lorch, E. (1969). *J. Phys. C*, **2**, 229–237.

McCarrol, W. H., Katz, L. & Ward, R. (1957). *J. Am. Chem. Soc.* **79**, 5410–5414.

McGrellis, S. A. (1994). Ph.D. thesis. University of Reading, England.

Soper, A. K., Howells, W. S. & Hannon, A. C. (1989). Report RAL-89-046. Rutherford Appleton Laboratory, Didcot, Oxford, England.

Torardi, C. C. & McCarley, R. E. (1985). *Inorg. Chem.* **24**, 476–481.